ACS APPLIED ENERGY MATERIALS
Cite This: ACS Appl. Energy Mater. XXXX, XXX, XXX−XXX
Article
www.acsaem.org

Scalable Synthesis of Size-Controlled Li_2S Nanocrystals for Next-Generation Battery Technologies

Yangzhi Zhao,[†] Yongan Yang,[*,‡] and Colin A. Wolden[*,†,§]

[†]Material Science Program, Colorado School of Mines, 1500 Illinois Street, Golden, Colorado 80401, United States
[‡]Institute of Molecular Plus, Tianjin University, No. 11 Building, No. 92 Weijin Road, Nankai District, Tianjin 300072, P. R. China
[§]Department of Chemical and Biological Engineering, Colorado School of Mines, 1613 Illinois Street, Golden, Colorado 80401, United States

Supporting Information

ABSTRACT: Lithium sulfide (Li_2S) nanocrystals (NCs) are critical materials for emerging solid-state and Li−S battery technologies. Conventional synthesis is energy intensive and costly, and offers limited size control. Here we describe a scalable approach wherein Li_2S is formed by contacting hydrogen sulfide (H_2S) gas with metalorganic solution at ambient temperature. NCs are recovered with essentially 100% yield in a subsequent evaporation step. Control of NC size and uniformity is demonstrated through manipulating parameters such as precursor concentration and solvent evaporation rate. A suite of complementary techniques confirm the production of anhydrous, phase-pure Li_2S nanocrystals with tunable size (5−20 nm) and narrow particle size distributions. Mild annealing conditions are identified to provide the purity necessary for battery applications, while retaining the original size distribution. Simple cathodes fabricated from the resulting NCs show promising battery performance, where the capacity approaches the theoretical value and displays good cyclability and rate capability.

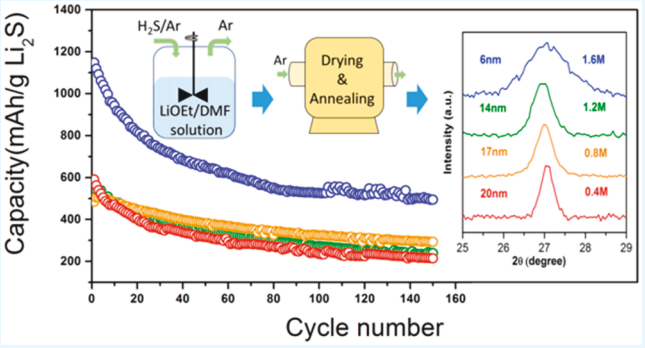

KEYWORDS: *lithium sulfide, size-controlled nanocrystals, scalable synthesis, annealing treatment, high initial capacity*

1. INTRODUCTION

The world is undergoing a quiet but rapid transformation in the way that energy is generated and consumed. Renewables such as solar and wind accounted for about two-thirds of new electricity capacity installed in 2016, and this fraction is expected to continue to grow.[1] One challenge with these resources is their temporal variation and the necessity for storage to efficiently dispatch them. Current energy storage options include mechanical (pumped hydropower, compressed air), thermal (latent heat), chemical (hydrogen, ammonia), and electrochemical (batteries).[2] Batteries are able to fulfill multiple roles in the energy storage system, and are particularly well-suited for short and moderate term electricity storage and power supply.[2−4] The Li-ion battery (LIB) is the leading rechargeable battery technology due to benefits such as portability, no memory effect, and low self-discharge.[2,5] In current LIBs a liquid electrolyte is sandwiched between a graphite anode and an intercalation-type metal oxide cathode (i.e., $LiCoO_2$, $LiMn_2O_4$, $LiFePO_4$).[6−8] This basic geometry is approaching its performance ceiling, and more advanced batteries with greater energy density are required to help expand deployment of technologies such as electric vehicles.[3,9−12] Lithium−sulfur (Li−S) and solid-state batteries are two alternative technologies that show promising charge capacity and energy density. Li−S is a conversion-type battery that follows a multiple electron conversion electrochemistry that enables very high specific capacity (1672 mA h/g S), 5−10 times greater than current technology.[9,10,13,14] Another benefit of sulfur is its earth abundance, which could significantly lower the cost. Solid-state electrolytes (SEs) can improve the capacity and safety of batteries by replacing the dense, flammable liquid electrolyte which accounts for a significant fraction of both weight and cost of Li-ion batteries.[15−17]

Li_2S is a crucial material for both Li−S battery and solid-state electrolyte fabrication. Li_2S cathodes present several advantages over sulfur since it is fully lithiated and does not need to accommodate the significant volume expansion (66−79%) that occurs in sulfur cathodes due to lithium insertion. Moreover, Li_2S cathode can be coupled with inexpensive lithium-free anode materials such as graphite, silicon, or tin. Therefore, safety issues caused by lithium dendrite growth on the Li anode may be mitigated. Sulfide glasses derived from $Li_2S−P_2S_5$[18] and related superionic conductors[19−21] are

Received: January 6, 2019
Accepted: February 11, 2019
Published: February 11, 2019

Downloaded via COLORADO SCHOOL OF MINES on March 1, 2019 at 18:48:40 (UTC).
See https://pubs.acs.org/sharingguidelines for options on how to legitimately share published articles.

© XXXX American Chemical Society

DOI: 10.1021/acsaem.9b00032
ACS Appl. Energy Mater. XXXX, XXX, XXX−XXX

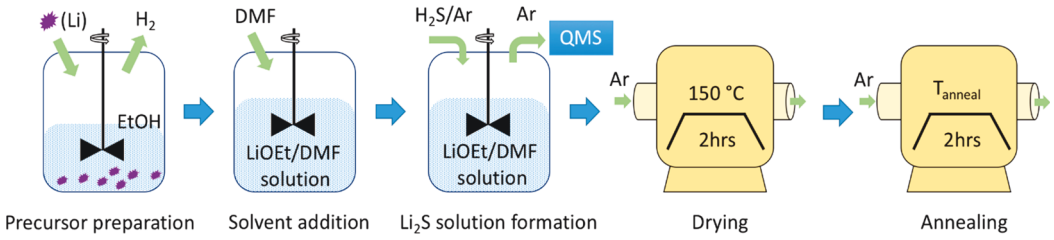

Figure 1. Schematic representation of solvent evaporation approach.

leading solid-state electrolytes with lithium-ion conductivity exceeding liquid electrolytes.[22,23] Li_2S is the key component and cost driver for these materials, which are typically produced by cold pressing and annealing. Sulfide glasses are more cost-effective and have much better mechanical properties than oxide alternatives such as perovskites.[20,24]

Anhydrous lithium sulfide is currently produced through endothermic carbothermal reduction reactions such as[25−28]

$$Li_2SO_{4(s)} + 2C_{(s)} \rightarrow Li_2S_{(s)} + 2CO_{2(g)}$$
$$\Delta G_m^{\ 0} \approx +120\ \text{kJ/mol} \quad (1)$$

$$Li_2CO_{3(s)} + H_2S_{(g)} \rightarrow Li_2S_{(s)} + H_2O_{(g)} + CO_{2(g)}$$
$$\Delta G_m^{\ 0} \approx +100\ \text{kJ/mol} \quad (2)$$

These high-temperature processes (600−1000 °C) produce Li_2S in the form of micropowders, and problems with purity and uniformity are concerned. Commercially available lithium sulfide consists of 30−100 μm sized particles that have poor electrochemical activity due to the large particle size.[29] Nanocrystals (NCs) are desirable for enhanced electrochemical performance since their increased specific surface area improves charge transfer and active material utilization.[5,28,30] For battery applications commercial Li_2S micropowders are commonly converted into nanoparticles by high-energy ball milling,[31−34] which is costly and time-consuming, and can introduce further impurities. In addition, there is limited control over the size, uniformity, or morphology of the final NCs. Thus, there is a critical need to develop alternative processes for scalable manufacturing of anhydrous metal sulfide nanocrystals.

Though nanomaterials possess extraordinary intrinsic properties, their practical deployment is often hindered by high synthesis costs driven by high-energy requirements and poor materials utilization.[35] There has been an increased emphasis on developing green manufacturing approaches.[36] Environmentally benign solvents, the absence of hazardous byproducts, and low energy budgets are among the key characteristics of a green synthetic strategy. Our group has recently developed a green approach to directly synthesize alkali metal sulfide NCs through reactive precipitation by contacting metalorganic precursor solutions with H_2S.[37] In this two-step process an alkoxide precursor is first made by reacting alkali metal (Li and Na) with alcohol, which is accompanied by the generation of valuable H_2:

$$2M_{(s)} + 2ROH_{(l)} \rightarrow 2ROM_{(sol)} + H_{2(g)}$$
$$\Delta G_m^{\ 0} \approx -265\ \text{kJ/mol} \quad (3)$$

Next, the alkoxide is diluted by addition of solvent to form a metalorganic solution (ROM). H_2S is then bubbled through the ROM solution, producing M_2S NCs (M = Li, and Na) through reactive precipitation with recovery of alcohol.

$$2ROM_{(sol)} + H_2S_{(g)} \rightarrow M_2S_{(s)} + 2ROH_{(l)}$$
$$\Delta G_m^{\ 0} \approx -116\ \text{kJ/mol} \quad (4)$$

The recovered alcohol can be recycled to make ROM solution again. The net result of the above two steps is as follows:

$$2M_{(s)} + H_2S_{(g)} \xrightarrow{RT,\,1\text{atm}} M_2S_{(s)} + H_{2(g)}$$
$$\Delta G_m^{\ 0} \approx -381\ \text{kJ/mol} \quad (5)$$

Our innovative process adheres to these tenets of green chemistry[38] and engineering.[39] Two valuable products, M_2S NCs (M = Li, and Na) and H_2, are successfully synthesized while simultaneously achieving complete abatement of a hazardous chemical (H_2S). The reactions above proceed with practically 100% atom economy, meaning that the alkali metal is fully converted to M_2S, and hydrogen is fully recovered from H_2S. These reactions are performed at ambient temperature and atmospheric pressure requiring minimal energy input due to the favorable reaction kinetics and thermodynamics. The M_2S NCs can be easily separated and collected by simple centrifugation as they are precipitated out of the solution. Likewise, H_2 is also easily collected since it is the only gaseous species in reaction 3. Moreover, we recently demonstrated the use of bubble columns as an effective approach for scalable manufacturing of these nanomaterials.[40]

Finally, a comment on the economics of the process is discussed herein. The use of lithium as a reagent may give one pause; however, Li is required in all advanced battery technologies, and its elemental form provides the highest purity at the lowest cost. Bulk lithium is most commonly traded in the form of lithium carbonate (the precursor for LIB cathodes) at ~$10/kg. The bulk price of elemental Li metal is ~$100/kg.[41] Using our approach 1 kg of lithium metal can be converted into 3.3 kg of Li_2S NCs. Thus, $100 worth of Li may be transformed into Li_2S NCs that retail for >$17,700,[42] over a 100-fold increase. Moreover, as noted above commercial Li_2S exists in the form of micropowders that require further processing to form NCs. The above analysis is quite simplistic, but provides some rationale for the economic potential of such a process.

Despite the advantages of reactive precipitation, a number of challenges remain, particularly for the Li_2S system. The number of alcohol/solvent combinations is limited, and flakes produced are not an ideal morphology.[43] Second, in the reactive precipitation process only ~85% of the Li_2S produced is directly recovered, with losses due to handling and dissolution in the alcohol. As lithium is the major cost driver, it is imperative to improve its utilization and product yield. Moreover, efforts to increase concentration, and thus

DOI: 10.1021/acsaem.9b00032
ACS Appl. Energy Mater. XXXX, XXX, XXX−XXX

throughput, have been complicated by clogging of reactor sparger during the reaction due to fast particle nucleation and growth. Cathodes made from Li_2S by reactive precipitation demonstrated high capacity (~700 mA h/g Li_2S) that is superior to ones made from commercial Li_2S.[44] However, this value remains well short of its theoretical capacity of 1166 mA h/g. It is hypothesized that performance was limited by the size of the NCs, which was ~100 nm.

In this study, a variation on the established chemistry has been adopted to address these issues. Instead of reactive precipitation, the synthesized Li_2S remains fully dissolved in solution when using the *N*,*N*-dimethylformamide (DMF) as the solvent. The first three steps are identical to our previous approach (Figure 1). In this case NCs were recovered via solvent evaporation. Although this introduces an additional step, advantages include nominally complete recovery of the valuable alkali metal and a broader process window with which to operate. We also explored the impact of annealing the recovered NCs prior to cathode formation.

NC size may be manipulated by the degree of supersaturation by adjusting the concentration of the ethoxide precursor solution and the heating rate of the furnace used for evaporation. Using this route anhydrous Li_2S NCs with reduced size and improved morphology were produced. The precipitate-free solution eliminates problems with sparger clogging, which enables increased concentration and throughput. This approach may also facilitate the synthesis of hierarchical Li_2S-shell structures for advanced cathode fabrication through the introduction of appropriate precursors for NC encapsulation.[45−49]

2. EXPERIMENTAL SECTION

2.1. Reagents. Ethanol (EtOH, CH_3CH_2OH, anhydrous, ≥99.5%), *N*,*N*-dimethylformamide (DMF, $HCON(CH_3)_2$, anhydrous, 99.8%), *N*-methyl-2-pyrrolidone (NMP, C_5H_9NO, 99.5%), bis(trifluoromethane)-sulfonimide [LiTFSI, $(CF_3SO_2)_2NLi$, 99.95%], and tetra(ethylene glycol) dimethyl ether [TEGDME, $CH_3O-(CH_2CH_2O)_4CH_3$, 99%] were purchased from Sigma-Aldrich. Lithium foil (Li, 0.75 mm thick ×19 mm wide, 99.9% trace metals basis) was purchased from Alfa Aesar. Acetylene black (AB; 35−45 nm), poly(vinylidene fluoride) [PVDF,$-(C_2H_2F_2)_n-$, >99.5%], and copper foil (99.99%, 9 μm) were purchased from MTI Corp. AB and PVDF were vacuum-dried in an oven at 60 °C for 16 h before being transferred in a glovebox. A specialty mixture of 10% of H_2S in Ar (Scott Specialty Gasses) and UHP grade argon gases were employed. The surface of lithium foil was carefully scratched to remove possible oxide film before using. All other chemicals were used as received.

2.2. Synthesis of Li_2S. The lithium ethoxide reagent was prepared in an Ar-filled glovebox (MBraun LABstar MB10 compact) by completely reacting lithium with ethanol on 1:8 molar ratio of Li:ethanol. Solvent DMF was added in an appropriate amount to make lithium ethoxide/DMF solution with desired concentration (0.4, 0.8, 1.2, and 1.6 M). The as-prepared solution was immediately transferred into a Parr reactor (model 4793) and sealed. The Parr reactor was then connected to the gas deliver/handling system in a fume hood. An illustration of the experimental setup can be found in our previous paper.[44] The gas lines were evacuated to the base pressure of the mechanical pump (<30 mTorr), and the leak rate was tested to ensure the vacuum integrity of the system. Before reaction starts, both H_2S/Ar mixture and diluent Ar were delivered at a flow rate of 40 sccm through the bypass to set a baseline reading of quadrupole mass spectrometer (QMS, Stanford Research Systems RGA300) in which effluent was online detected. To trigger the reaction, the bypass was closed, and both H_2S/Ar and diluent Ar were allowed to flow through the reactor with a timer being set up at the same time. H_2S/Ar was turned off when lithium ethoxide is fully reacted to reaction stoichiometry. At that time, diluent Ar was allowed to continue flowing for about 1 min before the inlet and outlet valves of the reactor were closed simultaneously. The sealed reactor was taken back in the Ar-filled glovebox before being opened up. Solvent evaporation was undertaken in a quartz tube furnace with a temperature controller to recover Li_2S NCs. Air was excluded through the drying process with continuous flow of UHP Ar.

2.3. Materials Characterization. X-ray diffraction (XRD) measurement was conducted on a Philips X'Pert X-ray diffractometer using Cu Kα radiation (λ = 0.154 05 nm). Samples were prepared in the Ar-filled glovebox by spreading sample powders onto glass slides. A drop of mineral oil was used to isolate the sample from hazard moisture in the air during the measurements. The background signal from glass slide and the mineral oil (a smooth and broad peak centered at 17.2° spanning from 10° to 25°) was later subtracted. Field emission scanning electron microscopy (FESEM) images were collected on a JEOL JSM-7000F FESEM instrument. The FESEM sample was prepared by first dispersing sample powder in hexane. A few drops of dispersion hexane solution were added onto a silicon wafer substrate on which sample powder was mounted after hexane was evaporated. Silicon wafer substrate was then immobilized onto an aluminum stub by using a double-sided carbon tape. An accelerating voltage of 5 kV was used for taking the SEM image. Thermogravimetric analysis (TGA) was performed on a Q50 TGA instrument. Before running, the alumina pan where sample is loaded was cleaned by isothermal treatment at 800 °C for 10 min. During experimental measurement, the flow rates of nitrogen were set at 40 and 60 mL/min for the balance compartment and the sample compartment, respectively. The measurement process was programmed to ramp from room temperature to desired temperature (150, 200, 250, and 300 °C) at a constant ramping rate of 2 °C/min, and then isotherm at each temperature for >12 h. Small angle X-ray scattering (SAXS) measurement was carried out under vacuum using a line collimation SAXS instrument supplied by Anton Paar. The instrument is equipped with a PW3830 stand-alone laboratory X-ray source from PANalytical, SAXSess camera from Anton Paar, and cyclone-imaging-plate reader from PerkinElmer. The X-ray is generated from a sealed-tube Cu anode ($\lambda_{Cu\text{-}K\alpha}$ = 0.154 nm) at operating conditions of 40 kV and 50 mA. The particle size distribution (PSD) results were obtained by processing initial data through three software packages: OptiQuant, SAXSquant, and Igor Pro, including procedures like background subtraction, transmission correction, data desmearing, and particle distribution analysis, etc. To mitigate the effect of small voids among primary particles, a homogeneous dispersion solution with 10 vol % was made by dispersing sample powder in 1,4-dioxane. About a 26 μL dispersion solution was loaded into a specially designed liquid sample holder for each measurement. The sample preparation and loading processes were performed in an Ar-filled glovebox. Sample has been ground by mortar and pestle prior to each measurement for all of the above techniques.

2.4. Electrochemical Test. To evaluate electrochemical performance of the resulting NCs, active material Li_2S NCs (40%) with acetylene black (45%) and PVDF binder (15%) were mixed by mortar and pestle. Then, an appropriate amount of *N*-methyl-2-pyrrolidone (NMP) was added to make slurry. The slurry was homogeneously cast on aluminum foil, and was dried to form electrode thin film by heating on hot plate at 100 °C overnight. The 10 mm size electrode discs were then cut from the as-dried film, and the mass loading of each disc was about 1.0 mg/cm^2. The half-cell batteries were assembled in a Swagelok cell using 2 M LiTFSI in TEGDME as the electrolyte, polypropylene membrane as separator, and Li foil as the anode. Electrode fabrication and cell assembly were performed in the glovebox with both O_2 and H_2O level <1.0 ppm. Cyclability was evaluated by galvanostatic charging/discharging battery in an electrochemical window between 1.5 and 3.0 V and with a rate of C/10. Cathodes were activated by charging the cell to 3.5 V on the first cycle. The rate test was conducted following a rate program from C/10 increasing to 2C and then decreasing to C/2, with each step of 6 cycles. All C-rates were calculated based on theoretical capacity value of Li_2S (1C = 1166 mA/g).

DOI: 10.1021/acsaem.9b00032
ACS Appl. Energy Mater. XXXX, XXX, XXX−XXX

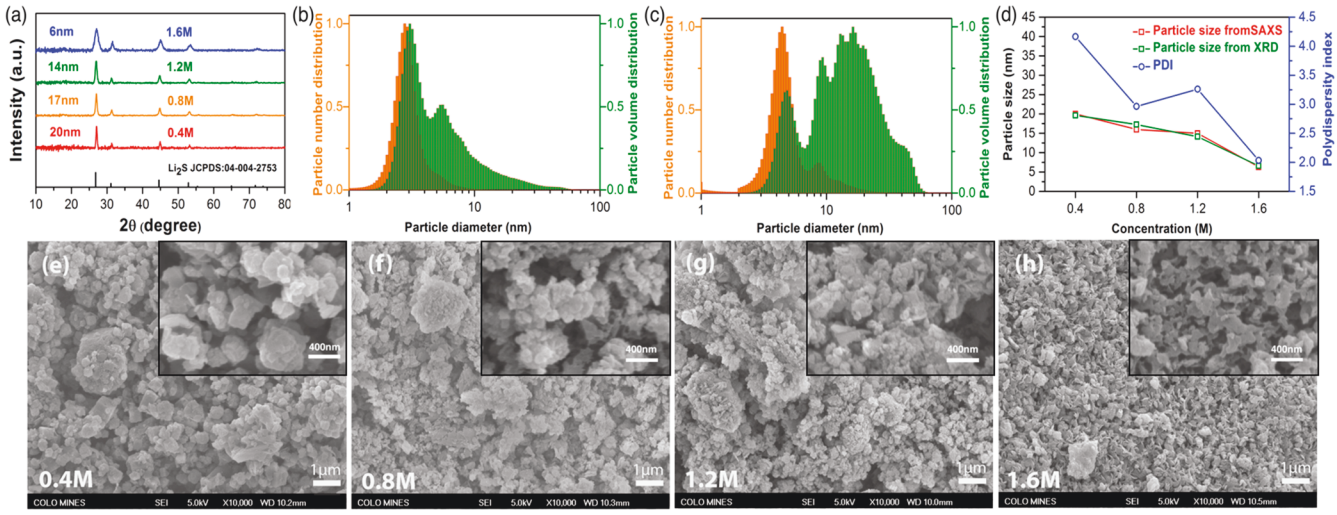

Figure 2. (a) XRD patterns of as-synthesized Li_2S NCs as a function of solution concentration. (b) PSDs based on number and volume extracted from SAXS for the 1.6 M sample. (c) PSDs from the 0.8 M sample. (d) Mean particle size extracted from XRD, SAXS, and polydispersity index as a function of solution concentration. (e–h) SEM images (10 000×) of Li_2S NCs as a function of solution concentration, with an inset of higher magnification (30 000×).

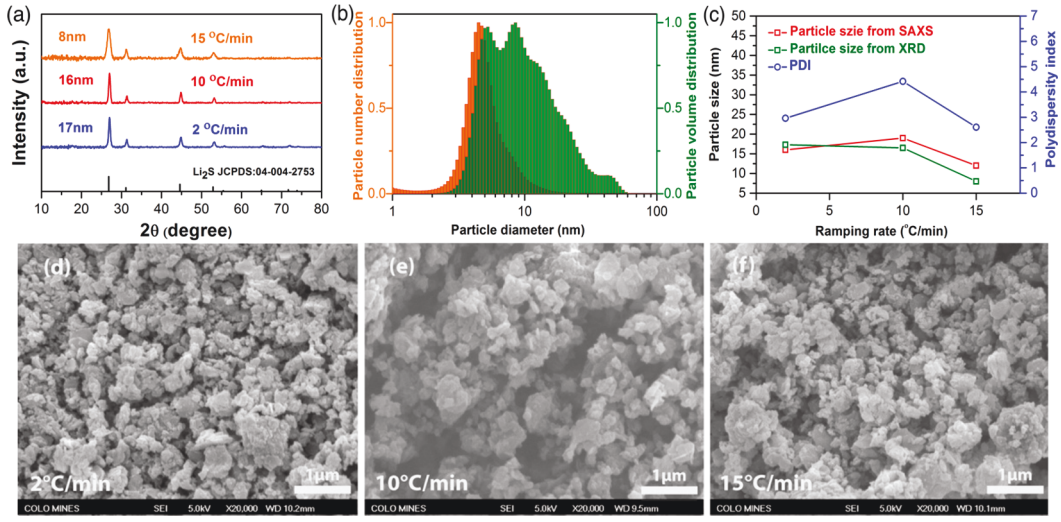

Figure 3. (a) XRD patterns of as-synthesized Li_2S NCs as a function of heating rate for the 0.8 M solution. (b) PSD extracted from SAXS for the 15 °C/min sample. (c) Mean particle size extracted from XRD, SAXS, and polydispersity index as a function of ramp rate. (d–f) SEM images (20 000×) of Li_2S NCs as a function of ramp rate for the 0.8 M solution.

3. RESULTS AND DISCUSSION

3.1. Size Control via Precursor Concentration. The first variable examined was the impact of the concentration of the lithium ethoxide solution on the size of as-synthesized NCs obtained after drying. Figure 2a shows wide angle XRD of the as-synthesized NCs as a function of ethoxide solution concentration. In all cases the material is crystalline, and there is no evidence of any impurity phases. As the concentration increases the peaks systematically broaden, reflecting a reduction in crystallite size. To quantify the particle size distribution (PSD) we performed SAXS as shown in Figure 2b,c and Figure S1a,b. A narrow PSD is obtained for the 1.6 M sample with average values of 3.1 and 6.3 nm based on particle number and volume, respectively. The polydispersity index (PDI) is defined as the ratio of mean size based on particle volume and number, and is typically used in polymer science to measure uniformity of molecular weight distribution.[50] The PSDs of NCs synthesized at lower concentration are broader (Figure 2c and Figure S1a,b), and the PDI decreases from 4 to 2 as the concentration was increased (Figure 2d). The mean size decreased from 20 to 6 nm as the concentration was increased from 0.4 to 1.6 M. The NC size obtained using XRD and the Scherrer equation agrees very well with mean particle size based on volume in SAXS (Figure 2d) as would be expected at this size range.[51] SEM analysis (Figure 2e–h) shows that these NCs aggregated into clusters are hundreds of nm in size. The morphology is much improved over the flakes obtained previously, and the size of the aggregates scales with concentration (100–600 nm). As with primary particle size the aggregates formed from the 1.6 M solution are considerably smaller than the lower concentrations, whose morphologies are quite similar. In this process NCs are formed during solvent evaporation, and it is hypothesized that the increased degree of supersaturation at higher concentrations leads to faster nucleation resulting in smaller particles.[43,52] It is notable that the 1.6 M solution that

DOI: 10.1021/acsaem.9b00032
ACS Appl. Energy Mater. XXXX, XXX, XXX–XXX

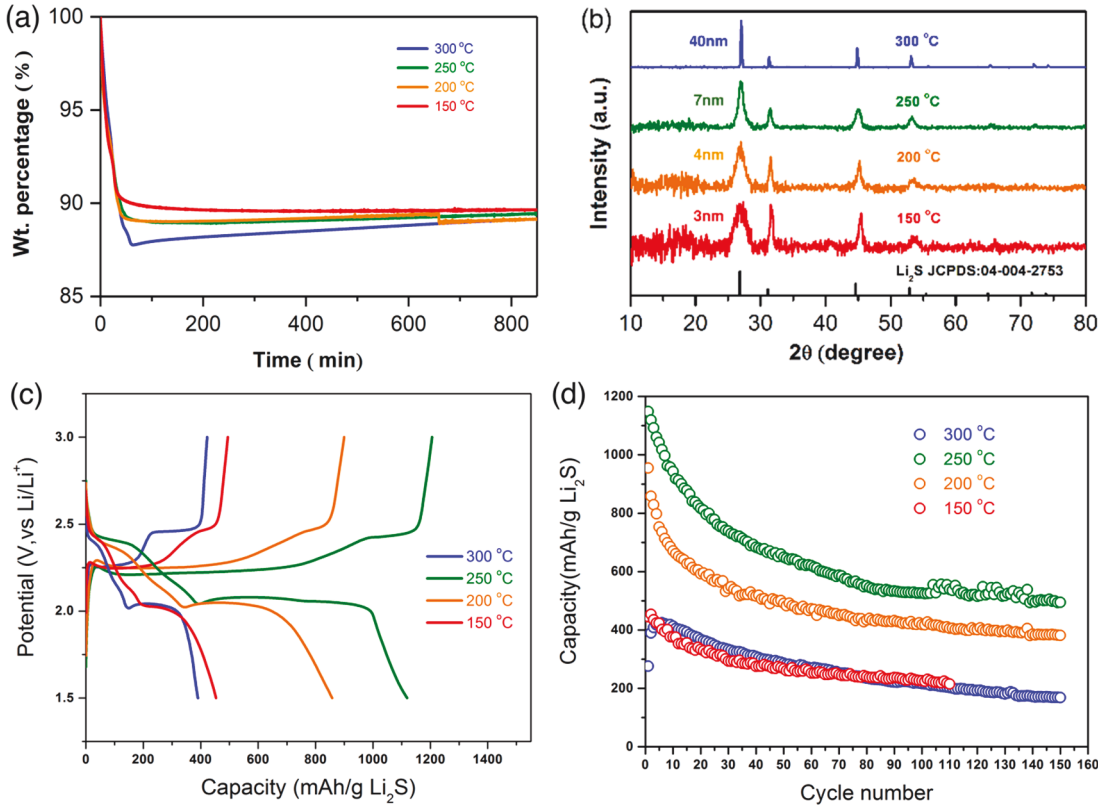

Figure 4. (a) Isothermal TGA scans and (b) resulting XRD patterns obtained from Li_2S NCs synthesized from 1.6 M solution and annealed at various temperatures. (c) Voltage profiles from charge/discharge and (d) cycling stability (based on discharge capacity) of cathodes fabricated with Li_2S NCs synthesized from 1.6 M solution as a function of annealing temperature.

produced the smallest particles is approaching the saturation limit.

3.2. Size Control via Heating Rate of Furnace. To further investigate the size control of NCs, the heating rate of the drying furnace was varied, with the hypothesis that faster ramps would more rapidly increase the degree of supersaturation, reducing the particle size. The previous work employed a heating rate of 2 °C/min. In this series the concentration was fixed at the intermediate value of 0.8 M , and the heating rate was varied from 2 to 15 °C/min. Figure 3 and Figure S1c summarize the resulting size and morphology as by XRD, SAXS, and SEM. XRD patterns of the material recovered at 2 and 10 °C/min are quite similar, with some degree of peak broadening observed at the highest heating rate of 15 °C/min. The SAXS data again is in good agreement with the XRD. PDI values ranged from 2.5 to 4, indicating comparable uniformity among different heating rates. SEM images (Figure 3d–f) demonstrate granular morphology of aggregates in 200–500 nm size. This manifests that heating rate has a minor impact on final particle size, but not as dramatically as concentration.

3.3. Study of Mild Annealing and Electrochemical Performance. It was found that cathodes produced from as-synthesized NCs dried at 150 °C for 2 h had very poor electrochemical performance. Although no impurities were observed in XRD, it was hypothesized that there may be residual solvent contamination. To test this hypothesis thermogravimetric analysis (TGA) on the as-synthesized 1.6 M sample was performed. Figure 4a displays TGA profiles as a function of time for 4 different annealing temperatures. All samples experienced a 10–11% reduction in mass during annealing, confirming the presence of impurities. At T = 150 °C, over 10 h was required before the mass stabilized, supporting why material dried for 2 h resulted in poor performance. Annealing at 200 and 250 °C thermal processes show very similar behavior, and both samples were stabilized within 2 h. The 300 °C treatment exhibits an overshoot and recovery. Interestingly, a very similar phenomenon was reported by Wang et al., who fabricated cathodes by impregnating graphene oxide with Li_2S dissolved in ethanol.[53] They speculated that the weight loss during annealing was due to decomposition of the solvated compound $Li_2S\cdot CH_3CH_2OH$. They also suggested that this compound is electrochemically inactive and must be removed by annealing at 200 °C or above to achieve optimum battery performance.[53]

One concern with postannealing is that NCs may increase in size through Oswald ripening,[54,55] thereby nullifying the size control exhibited above. Figure 4b compares XRD patterns of as-synthesized NCs obtained from a 1.6 M solution after drying at 150 °C and with powders subsequently annealed at 200, 250, and 300 °C for 2 h. The peak width decreases very modestly up to 250 °C, suggesting that the NC size was not impacted significantly. Estimates of crystal size using the Scherrer equation indicate 3, 4, and 7 nm for samples annealed at 150, 200, and 250 °C, respectively. In addition, the background noise is significantly reduced as the annealing temperature was increased from 150 to 250 °C, suggesting there is an improvement in crystallinity. In contrast, material annealed at 300 °C displays very sharp peaks, indicative of significant NC growth and coalescence. The Scherrer analysis suggests that the particle size jumps to ~40 nm.

DOI: 10.1021/acsaem.9b00032
ACS Appl. Energy Mater. XXXX, XXX, XXX–XXX

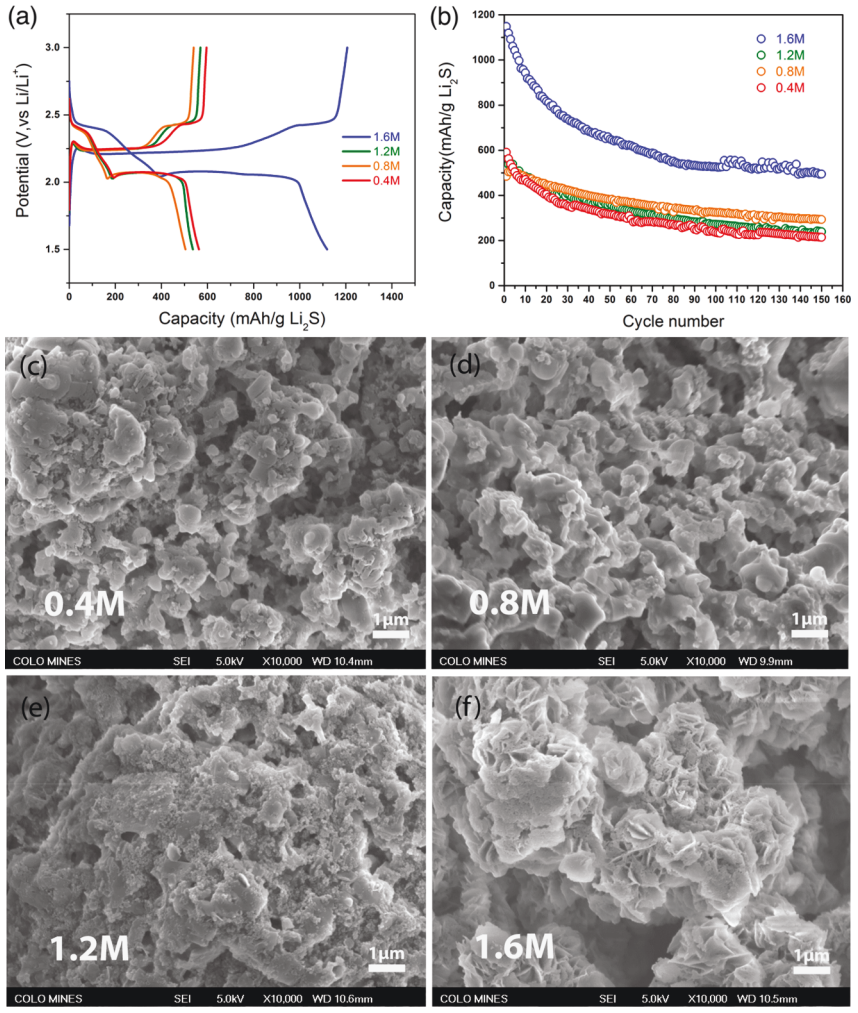

Figure 5. (a) Voltage profiles from charge/discharge and (b) cyclability (based on discharge capacity) of cathodes fabricated with Li_2S NCs annealed at T = 250 °C as a function of solution concentration. (c–f) SEM images (10,000X) for 250 °C postannealing samples as a function of concentration.

The electrochemical performances of the synthesized Li_2S NCs were assessed by fabricating cathodes from mixtures of Li_2S (40 wt %), acetylene black (45 wt %), and PVDF binder (15 wt %) using the standard slurry method. The electrochemical performance correlated very well with the annealing results described above. Figure 4c shows typical voltage profiles obtained from Li_2S cathodes fabricated from 1.6 M solution and annealed at different temperatures. The activation curve of the first charging cycle was omitted because it goes slightly beyond theoretical capacity value of Li_2S, with the excess charge attributed to decomposition of liquid electrolyte and the formation of a surface electrolyte interface (SEI) layer.[56−58] Figure 4d displays the cycling stability of these cathodes at C/10. The performance using material annealed at both 150 and 300 °C is very poor, albeit for different reasons. The poor capacity observed at T = 150 °C is attributed to the presence of impurities as discussed above, while at T = 300 °C the initial performance is very bad and actually improves during the first several cycles before declining. It is suggested that the initial improvement is due to cycling breaking up the large NCs produced during annealing, exposing more active material. However, this benefit is confined to the first half dozen cycles after which performance degrades. Cathodes fabricated from material annealed at 200 °C displayed greatly improved performance, and the sample annealed at T = 250 °C achieved an initial discharge capacity of 1148 mA h/g, which is 98.5% of the theoretical value. Capacity decays at a slow rate (~0.4% per cycle) and begins to stabilize at ~500 mA h/g after 130 cycles. The superior performance of the 250 °C relative to the 200 °C is attributed to the improved crystallinity observed in XRD. The improved crystallinity may reduce the impedance for lithium-ion transportation.[59]

The importance of size was confirmed by comparing the performance of cathodes using NCs produced as a function of solution concentration. In each case these NCs were annealed at the optimal temperature of T = 250 °C. Likewise, Figure 5a,b compares the voltage profiles and cycling stability of cathodes as a function of concentration. Cathodes using Li_2S synthesized at 1.6 M showcased superior performance, whereas at 0.4−1.2 M all displayed very similar performance which was comparable to NCs produced by reactive precipitation.[44] This is consistent with the physical characterization described above. In terms of XRD and SEM the 1.6 M derived NCs are clearly distinct from other solutions with regard to size, uniformity, and morphology. The morphology of the material annealed at T = 250 °C is very similar among the samples obtained in the 0.4−1.2 M concentration range (Figure 5c−e). The 1.6 M sample forms a porous nanoflower morphology

DOI: 10.1021/acsaem.9b00032
ACS Appl. Energy Mater. XXXX, XXX, XXX−XXX

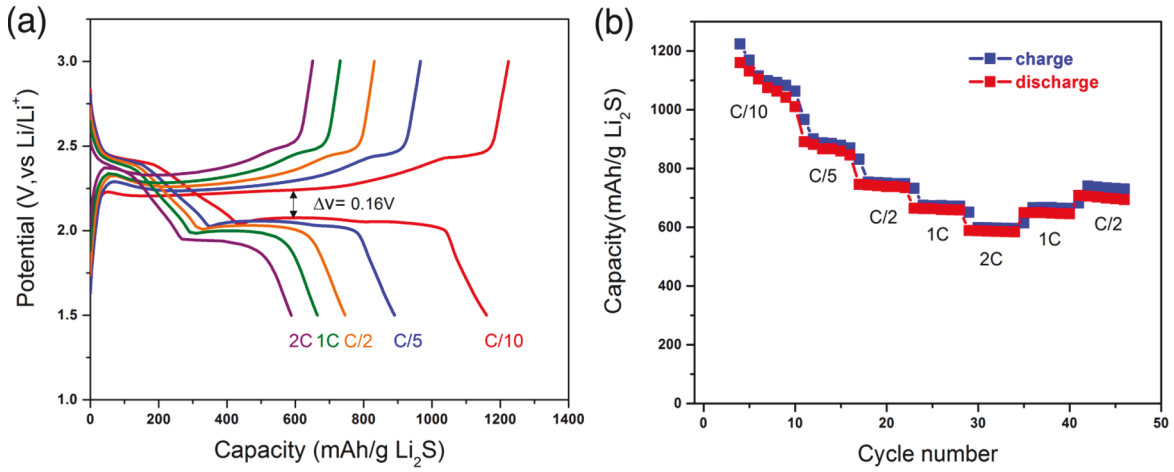

Figure 6. (a) Voltage profiles and (b) charge/discharge capacity of cathodes fabricated with Li_2S NCs synthesized from 1.6 M solution as a function of C-rates.

with thin petals as opposed to clustered aggregates. The step change in cathode performance is attributed to this unique morphology, which enables Li_2S to be fully utilized during cycling. There are several reasons why electrodes made from smaller NCs delivered better performance. Ionic conductance is improved due to the reduction in diffusion lengths. Moreover, the increased specific surface area improves charge transfer and active material utilization.[30,59] Although small NCs are more useful in cathode application, it does not mean bigger particles have no use at all. The ability to tune NC size may be important for other applications such as solid-state electrolyte formation.

Table S1 provides a comparison to the relevant literature arranged from top to bottom by magnitude of the initial discharge capacity. Among these reports our cathodes display the highest initial capacity and reasonable stability even when compared to some cathodes with sophisticated encapsulation strategies or employing electrolyte additives. For instance, to mitigate the impact of polysulfide dissolution and shuttling, Li_2S has been embedded into a carbon matrix during cathode fabrication, with examples including carbon nanotubes, nanofibers, graphene, or reduced graphene oxide (rGO).[53,60−64] Others formed Li_2S@C hybrid structures through chemical vapor deposition or solution-based approaches.[5,30,62,65] A third approach has been to form Li_2S/C composites through high-energy ball milling.[28,65,66] Recently, Wu et al.[48] developed a $LiTiO_2$ encapsulation strategy which reduced the initial capacity but displayed remarkable stability at C/2 rates. Another common approach to mitigate the polysulfide shuttle is through the use of additives such as $LiNO_3$,[53,60−62,65−67] LiI,[30,48] or polysulfides (Li_2S_6 or Li_2S_8)[5,28,53,60] in the electrolyte solution. Note that almost all of these high-performance cathodes employed high-temperature (600−1500 °C) processing steps during their fabrication. Relative to these leading reports our cathodes fabricated from sub-10 nm NCs displayed the highest initial discharge capacity. It is also a dramatic improvement over our previous work using Li_2S NCs fabricated by reactive precipitation.[44] As the annealing and cathode fabrication steps were nominally identical, the improvements are attributed to the reduced NC size. Though stability was inferior to most reports, it was quite respectable considering the absence of encapsulation or the use of additives. As a solution-based approach it is amenable to the introduction of encapsulation compounds as described in the literature,[5,30] and this is something we plan to address in future work.

To further assess performance, the rate capability of the 1.6 M-based cathode was evaluated at different rates from C/10 to 2C as shown in Figure 6. A very small voltage hysteresis ΔV = 0.16 V is observed for the C/10 voltage profile as opposed to the usually reported 0.2−0.4 V,[48,66,68,69] which is a reflection of improved electronic conductivity and Li ionic diffusivity due to the reduced particle size.[5,44,68] In Figure 6b, the sample displays a capacity of ∼870, 740, 670, and 590 mA h/g as the cycling rate is increased to C/5, C/2, 1C, and 2C, respectively. These results compare very favorably with leading reports in the literature. For example, at the 2C-rate and a similar number of cycles Yushin's group reported ∼450 mA h/g for both hierarchical carbon-coated[30] and $LiTiO_2$-encapsulated[48] cathodes. More importantly, the capacity of our battery remains ∼660 mA h/g at 1C and ∼715 mA h/g at C/2 in return cycles, which is 98.5% and 96.6% retention, respectively, indicating a good reversibility. In short, such small voltage hysteresis and good rate performance are again attributed to the small size and high purity of NCs produced in this work.

4. CONCLUSIONS

In summary, we have reported an alternative approach for scalable synthesis of Li_2S NCs, where the use of DMF solvent suppresses the precipitation of Li_2S in the resultant solution. This approach provides new capabilities in addition to benefits H_2 cogeneration and H_2S abatement as in our previous methods. Specifically, the solvation/evaporation approach enables nearly 100% atom efficiency of lithium and controllable size/uniformity of the produced NCs through manipulation of solution supersaturation. Modest annealing conditions were identified that improve purity and crystallinity while retaining size. Cathodes fabricated using these Li_2S NCs obtained 98.5% of theoretical capacity as well as promising cyclability and rate capability, which is among the best performance reported to date for Li_2S cathodes fabricated by simply mixing sulfide with common binder and carbon additives. Overall, the process−structure−property−performance relationship in these systems has been successfully established, where promising cathode performance stems from ultrasmall NPs (5−6 nm) with excellent crystallinity

DOI: 10.1021/acsaem.9b00032
ACS Appl. Energy Mater. XXXX, XXX, XXX−XXX

out of 1.6 M concentration solution and after going through mild annealing at 250 °C. The results also exhibit the potential of our material to achieve much improved performance when integrating more advanced and sophisticated cathode design such as shell encapsulation, carbon matrix embedment, hierarchical-structure build up, and so on. This approach may also facilitate the synthesis of hierarchical Li_2S NC@ carbon structure for advanced cathode fabrication through the introduction of polymer precursors before solvent evaporation.

■ ASSOCIATED CONTENT

Supporting Information

The Supporting Information is available free of charge on the ACS Publications website at DOI: 10.1021/acsaem.9b00032.

SAXS data and table of comparison of cathode performance obtained in this work with the literature (PDF)

■ AUTHOR INFORMATION

Corresponding Authors

*E-mail: revned_yang@tju.edu.cn.
*E-mail: cwolden@mines.edu.

ORCID

Yongan Yang: 0000-0003-1451-2923
Colin A. Wolden: 0000-0001-6576-048X

Author Contributions

The manuscript was written through contributions of all authors. All authors have given approval to the final version of the manuscript.

Notes

The authors declare no competing financial interest.

■ ACKNOWLEDGMENTS

We acknowledge the US National Science Foundation for support of this work through Award 1825470. We also thank Prof. Don Williamson for his assistance in conducting and interpreting the SAXS measurements.

■ REFERENCES

(1) *Renewables 2017*; International Energy Agency, 2017.
(2) Evans, A.; Strezov, V.; Evans, T. J. Assessment of utility energy storage options for increased renewable energy penetration. *Renewable Sustainable Energy Rev.* **2012**, *16*, 4141−4147.
(3) Chen, H.; Cong, T. N.; Yang, W.; Tan, C.; Li, Y.; Ding, Y. Progress in electrical energy storage system: A critical review. *Prog. Nat. Sci.* **2009**, *19*, 291−312.
(4) Dunn, B.; Kamath, H.; Tarascon, J. M. Electrical Energy Storage for the Grid: A Battery of Choices. *Science* **2011**, *334*, 928−935.
(5) Wu, F.; Kim, H.; Magasinski, A.; Lee, J. T.; Lin, H.-T.; Yushin, G. Harnessing Steric Separation of Freshly Nucleated Li_2S Nanoparticles for Bottom-Up Assembly of High-Performance Cathodes for Lithium-Sulfur and Lithium-Ion Batteries. *Adv. Energy Mater.* **2014**, *4*, 1400196.
(6) Scrosati, B. Lithium Rocking Chair Batteries: An old Concept? *J. Electrochem. Soc.* **1992**, *139*, 2776−2781.
(7) Adelhelm, P.; Hartmann, P.; Bender, C. L.; Busche, M.; Eufinger, C.; Janek, J. From lithium to sodium: cell chemistry of room temperature sodium-air and sodium-sulfur batteries. *Beilstein J. Nanotechnol.* **2015**, *6*, 1016−1055.
(8) Dahbi, M.; Ghamouss, F.; Tran-Van, F.; Lemordant, D.; Anouti, M. Comparative study of EC/DMC LiTFSI and $LiPF_6$ electrolytes for electrochemical storage. *J. Power Sources* **2011**, *196*, 9743−9750.
(9) Song, M. K.; Cairns, E. J.; Zhang, Y. Lithium/sulfur batteries with high specific energy: old challenges and new opportunities. *Nanoscale* **2013**, *5*, 2186−2204.
(10) Yin, Y. X.; Xin, S.; Guo, Y. G.; Wan, L. J. Lithium-sulfur batteries: electrochemistry, materials, and prospects. *Angew. Chem., Int. Ed.* **2013**, *52*, 13186−13200.
(11) Grey, C. P.; Tarascon, J. M. Sustainability and in situ monitoring in battery development. *Nat. Mater.* **2017**, *16*, 45−56.
(12) Bruce, P. G.; Freunberger, S. A.; Hardwick, L. J.; Tarascon, J. M. Li-O_2 and Li-S batteries with high energy storage. *Nat. Mater.* **2012**, *11*, 19−29.
(13) Liang, C.; Dudney, N. J.; Howe, J. Y. Hierarchically Structured Sulfur/Carbon Nanocomposite Material for High-Energy Lithium Battery. *Chem. Mater.* **2009**, *21*, 4724−4730.
(14) Liang, S.; Xia, Y.; Liang, C.; Gan, Y.; Huang, H.; Zhang, J.; Tao, X.; Sun, W.; Han, W.; Zhang, W. A green and facile strategy for the low-temperature and rapid synthesis of Li_2S@PC−CNT cathodes with high Li_2S content for advanced Li−S batteries. *J. Mater. Chem. A* **2018**, *6*, 9906−9914.
(15) Wood, D. L.; Li, J.; Daniel, C. Prospects for reducing the processing cost of lithium ion batteries. *J. Power Sources* **2015**, *275*, 234−242.
(16) Fang, X.; Peng, H. A revolution in electrodes: recent progress in rechargeable lithium-sulfur batteries. *Small* **2015**, *11*, 1488−1511.
(17) Judez, X.; Zhang, H.; Li, C.; Eshetu, G. G.; González-Marcos, J. A.; Armand, M.; Rodriguez-Martinez, L. M. Review—Solid Electrolytes for Safe and High Energy Density Lithium-Sulfur Batteries: Promises and Challenges. *J. Electrochem. Soc.* **2018**, *165*, A6008−A6016.
(18) Seino, Y.; Ota, T.; Takada, K.; Hayashi, A.; Tatsumisago, M. A sulphide lithium super ion conductor is superior to liquid ion conductors for use in rechargeable batteries. *Energy Environ. Sci.* **2014**, *7*, 627−631.
(19) Kato, Y.; Hori, S.; Saito, T.; Suzuki, K.; Hirayama, M.; Mitsui, A.; Yonemura, M.; Iba, H.; Kanno, R. High-power all-solid-state batteries using sulfide superionic conductors. *Nature Energy* **2016**, *1*, 16030.
(20) Kamaya, N.; Homma, K.; Yamakawa, Y.; Hirayama, M.; Kanno, R.; Yonemura, M.; Kamiyama, T.; Kato, Y.; Hama, S.; Kawamoto, K.; Mitsui, A. A lithium superionic conductor. *Nat. Mater.* **2011**, *10*, 682−686.
(21) Chu, I. H.; Nguyen, H.; Hy, S.; Lin, Y. C.; Wang, Z.; Xu, Z.; Deng, Z.; Meng, Y. S.; Ong, S. P. Insights into the Performance Limits of the $Li_7P_3S_{11}$ Superionic Conductor: A Combined First-Principles and Experimental Study. *ACS Appl. Mater. Interfaces* **2016**, *8*, 7843−7853.
(22) Liu, Y.; He, P.; Zhou, H. Rechargeable Solid-State Li-Air and Li-S Batteries: Materials, Construction, and Challenges. *Adv. Energy Mater.* **2018**, *8*, 1701602.
(23) Busche, M. R.; Weber, D. A.; Schneider, Y.; Dietrich, C.; Wenzel, S.; Leichtweiss, T.; Schröder, D.; Zhang, W.; Weigand, H.; Walter, D.; Sedlmaier, S. J.; Houtarde, D.; Nazar, L. F.; Janek, J. In Situ Monitoring of Fast Li-Ion Conductor $Li_7P_3S_{11}$ Crystallization Inside a Hot-Press Setup. *Chem. Mater.* **2016**, *28*, 6152−6165.
(24) Minami, T.; Hayashi, A.; Tatsumisago, M. Recent progress of glass and glass-ceramics as solid electrolytes for lithium secondary batteries. *Solid State Ionics* **2006**, *177*, 2715−2720.
(25) Ikeda, N.; Yamamoto, K. Method of Manufacturing Lithium Sulfide. EP0802159 B1, 2001.
(26) Miyashita, N. Method for Producing Lithium Sulfide for Lithium Ion Cell Solid Electrolyte Material. U.S. Patent 20140037535 A1, 2014.
(27) Jacob, S. R.; Brown, P. M. Process for producing high purity lithium sulfide. U.S. Patent 4126666 A, 1978.
(28) Kohl, M.; Brückner, J.; Bauer, I.; Althues, H.; Kaskel, S. Synthesis of highly electrochemically active Li_2S nanoparticles for lithium−sulfur-batteries. *J. Mater. Chem. A* **2015**, *3*, 16307−16312.
(29) Nelson, J.; Misra, S.; Yang, Y.; Jackson, A.; Liu, Y.; Wang, H.; Dai, H.; Andrews, J. C.; Cui, Y.; Toney, M. F. In Operando X-ray

Diffraction and Transmission X-ray Microscopy of Lithium Sulfur Batteries. *J. Am. Chem. Soc.* **2012**, *134*, 6337−6343.
(30) Wu, F.; Lee, J. T.; Fan, F.; Nitta, N.; Kim, H.; Zhu, T.; Yushin, G. A Hierarchical Particle-Shell Architecture for Long-Term Cycle Stability of Li_2S Cathodes. *Adv. Mater.* **2015**, *27*, 5579−5586.
(31) Yang, Y.; Zheng, G.; Misra, S.; Nelson, J.; Toney, M. F.; Cui, Y. High-capacity micrometer-sized Li_2S particles as cathode materials for advanced rechargeable lithium-ion batteries. *J. Am. Chem. Soc.* **2012**, *134*, 15387−15394.
(32) Takeuchi, T.; Sakaebe, H.; Kageyama, H.; Senoh, H.; Sakai, T.; Tatsumi, K. Preparation of electrochemically active lithium sulfide-carbon composites using spark-plasma-sintering process. *J. Power Sources* **2010**, *195*, 2928−2934.
(33) Cai, K.; Song, M.-K. K.; Cairns, E. J.; Zhang, Y. Nanostructured Li_2S-C composites as cathode material for high-energy lithium/sulfur batteries. *Nano Lett.* **2012**, *12*, 6474−6479.
(34) Zhang, J.; Zhong, H.; Zheng, C.; Xia, Y.; Liang, C.; Huang, H.; Gan, Y.; Tao, X.; Zhang, W. All-solid-state batteries with slurry coated $LiNi_{0.8}Co_{0.1}Mn_{0.1O2}$ composite cathode and Li_6PS_5Cl electrolyte: Effect of binder content. *J. Power Sources* **2018**, *391*, 73−79.
(35) Anctil, A.; Babbitt, C. W.; Raffaelle, R. P.; Landi, B. J. Material and energy intensity of fullerene production. *Environ. Sci. Technol.* **2011**, *45*, 2353−2359.
(36) Patete, J. M.; Peng, X. H.; Koenigsmann, C.; Xu, Y.; Karn, B.; Wong, S. S. Viable methodologies for the synthesis of high-quality nanostructures. *Green Chem.* **2011**, *13*, 482−519.
(37) Li, X.; Zhao, Y.; Brennan, A.; McCeig, M.; Wolden, C. A.; Yang, Y. Reactive Precipitation of Anhydrous Alkali Sulfide Nanocrystals with Concomitant Abatement of Hydrogen Sulfide and Cogeneration of Hydrogen. *ChemSusChem* **2017**, *10*, 2904−2913.
(38) Anastas, P. T.; Warner, J. C. *Green Chemistry: Theory and Practice*; Oxford University Press: New York, 1998.
(39) Abraham, M. A.; Nguyen, N. Green Engineering: Defining principles. *Environ. Prog.* **2003**, *22*, 233−236.
(40) Hietala, K.; Zhao, Y.; Yang, Y.; Wolden, C. A. Scalable Synthesis of Alkali Sulfide Nanocrystals Using a Bubble Column Reactor. *Ind. Eng. Chem. Res.* **2018**, *57*, 8436−8442.
(41) Bradley, D.; Jaskula, B. *Lithium—For harnessing renewable energy*; U.S. Geological Survey Fact Sheet, 2014.
(42) Alfa-Aesar. https://www.alfa.com/en/catalog/012839/ (accessed July 25, 2018).
(43) Robinson, J. P.; Koenig, G. M. Tuning solution chemistry for morphology control of lithium-ion battery precursor particles. *Powder Technol.* **2015**, *284*, 225−230.
(44) Li, X.; Wolden, C. A.; Ban, C.; Yang, Y. Facile Synthesis of Lithium Sulfide Nanocrystals for Use in Advanced Rechargeable Batteries. *ACS Appl. Mater. Interfaces* **2015**, *7*, 28444−28451.
(45) Jeong, S.; Bresser, D.; Buchholz, D.; Winter, M.; Passerini, S. Carbon coated lithium sulfide particles for lithium battery cathodes. *J. Power Sources* **2013**, *235*, 220−225.
(46) Liang, S.; Liang, C.; Xia, Y.; Xu, H.; Huang, H.; Tao, X.; Gan, Y.; Zhang, W. Facile synthesis of porous Li_2S@C composites as cathode materials for lithium−sulfur batteries. *J. Power Sources* **2016**, *306*, 200−207.
(47) Ogoke, O.; Wu, G.; Wang, X.; Casimir, A.; Ma, L.; Wu, T.; Lu, J. Effective strategies for stabilizing sulfur for advanced lithium−sulfur batteries. *J. Mater. Chem. A* **2017**, *5*, 448−469.
(48) Wu, F.; Pollard, T. P.; Zhao, E.; Xiao, Y.; Olguin, M.; Borodin, O.; Yushin, G. Layered $LiTiO_2$ for the protection of Li_2S cathodes against dissolution: mechanisms of the remarkable performance boost. *Energy Environ. Sci.* **2018**, *11*, 807−817.
(49) Zhang, J.; Huang, H.; Bae, J.; Chung, S.-H.; Zhang, W.; Manthiram, A.; Yu, G. Nanostructured Host Materials for Trapping Sulfur in Rechargeable Li-S Batteries: Structure Design and Interfacial Chemistry. *Small Methods* **2018**, *2*, 1700279.
(50) Pradel, K. C.; Sohn, K.; Huang, J. Cross-flow purification of nanowires. *Angew. Chem., Int. Ed.* **2011**, *50*, 3412−3416.
(51) Borchert, H.; Shevchenko, E. V.; Robert, A.; Mekis, I.; Kornowski, A.; Grübel, G.; Weller, H. Determination of Nanocrystal Sizes: A Comparison of TEM, SAXS, and XRD Studies of Highly Monodisperse $CoPt_3$ Particles. *Langmuir* **2005**, *21*, 1931−1936.
(52) Oh, J.-M.; Hwang, S.-H.; Choy, J.-H. The effect of synthetic conditions on tailoring the size of hydrotalcite particles. *Solid State Ionics* **2002**, *151*, 285−291.
(53) Wang, C.; Wang, X.; Yang, Y.; Kushima, A.; Chen, J.; Huang, Y.; Li, J. Slurryless Li_2S/reduced graphene oxide cathode paper for high-performance lithium sulfur battery. *Nano Lett.* **2015**, *15*, 1796−1802.
(54) Capek, I. Radical polymerization of polar unsaturated monomers in direct microemulsion systems. *Adv. Colloid Interface Sci.* **1999**, *80*, 85−149.
(55) Xie, X.; Chen, S.; Ding, W.; Nie, Y.; Wei, Z. An extraordinarily stable catalyst: Pt NPs supported on two-dimensional $Ti_3C_2 \times 2$ (X = OH, F) nanosheets for oxygen reduction reaction. *Chem. Commun.* **2013**, *49*, 10112−10114.
(56) Chan, C. K.; Zhang, X. F.; Cui, Y. High Capacity Li Ion Battery Anodes Using Ge Nanowires. *Nano Lett.* **2008**, *8*, 307−309.
(57) Li, J.; Zhao, Y.; Wang, N.; Guan, L. A high performance carrier for SnO_2 nanoparticles used in lithium ion battery. *Chem. Commun.* **2011**, *47*, 5238−5240.
(58) Tarquini, G.; Di Carli, M.; Seta, L. D.; Moreno, M.; Prosini, P. P. Effectiveness of dioxolane/dimethoxyethane mixed solvent for the fabrication of lithium-sulfur semiflow batteries. *Solid State Ionics* **2018**, *317*, 170−174.
(59) Shen, Y.; Eltzholtz, J. R.; Iversen, B. B. Controlling Size, Crystallinity, and Electrochemical Performance of $Li_4Ti_5O_{12}$Nanocrystals. *Chem. Mater.* **2013**, *25*, 5023−5030.
(60) Han, K.; Shen, J.; Hayner, C. M.; Ye, H.; Kung, M. C.; Kung, H. H. Li_2S-reduced graphene oxide nanocomposites as cathode material for lithium sulfur batteries. *J. Power Sources* **2014**, *251*, 331−337.
(61) Wu, M.; Cui, Y.; Fu, Y. Li_2S Nanocrystals Confined in Free-Standing Carbon Paper for High Performance Lithium-Sulfur Batteries. *ACS Appl. Mater. Interfaces* **2015**, *7*, 21479−21486.
(62) Wang, D. H.; Xie, D.; Yang, T.; Zhong, Y.; Wang, X. L.; Xia, X. H.; Gu, C. D.; Tu, J. P. Li_2S@C composite incorporated into 3D reduced graphene oxide as a cathode material for lithium-sulfur batteries. *J. Power Sources* **2016**, *313*, 233−239.
(63) Wu, F.; Lee, J. T.; Magasinski, A.; Kim, H.; Yushin, G. Solution-Based Processing of Graphene-Li_2S Composite Cathodes for Lithium-Ion and Lithium-Sulfur Batteries. *Part. Part. Syst. Charact.* **2014**, *31*, 639−644.
(64) Wang, X.; Bi, X.; Wang, S.; Zhang, Y.; Du, H.; Lu, J. High-Rate and Long-Term Cycle Stability of Li-S Batteries Enabled by Li_2S/TiO_2-Impregnated Hollow Carbon Nanofiber Cathodes. *ACS Appl. Mater. Interfaces* **2018**, *10*, 16552−16560.
(65) Chen, L.; Liu, Y.; Zhang, F.; Liu, C.; Shaw, L. L. PVP-Assisted Synthesis of Uniform Carbon Coated Li_2S/CB for High-Performance Lithium-Sulfur Batteries. *ACS Appl. Mater. Interfaces* **2015**, *7*, 25748−25756.
(66) Liu, J.; Nara, H.; Yokoshima, T.; Momma, T.; Osaka, T. Li_2S cathode modified with polyvinylpyrrolidone and mechanical milling with carbon. *J. Power Sources* **2015**, *273*, 1136−1141.
(67) Yang, Y.; Zheng, G.; Misra, S.; Nelson, J.; Toney, M. F.; Cui, Y. High-capacity micrometer-sized Li_2S particles as cathode materials for advanced rechargeable lithium-ion batteries. *J. Am. Chem. Soc.* **2012**, *134*, 15387−15394.
(68) Yang, Y.; Zheng, G.; Cui, Y. Nanostructured sulfur cathodes. *Chem. Soc. Rev.* **2013**, *42*, 3018−3032.
(69) Zhang, J.; Shi, Y.; Ding, Y.; Peng, L.; Zhang, W.; Yu, G. A Conductive Molecular Framework Derived Li_2S/N,P-Codoped Carbon Cathode for Advanced Lithium-Sulfur Batteries. *Adv. Energy Mater.* **2017**, *7*, 1602876.

DOI: 10.1021/acsaem.9b00032
ACS Appl. Energy Mater. XXXX, XXX, XXX−XXX